https://doi.org/10.5194/nhess-2024-207
Preprint. Discussion started: 18 November 2024

Natural Hazards and Earth System Sciences
Discussions

Improving Pluvial Flood Simulations with Multi-source DEM Super-Resolution

Yue Zhu[1,6], Paolo Burlando[1], Puay Yok Tan[2], Christian Geiß[3,4], and Simone Fatichi[5]

[1]Institute of Environmental Engineering, ETH Zurich, Switzerland
[2]Department of Architecture, National University of Singapore, Singapore
[3]German Remote Sensing Data Center (DFD), German Aerospace Center (DLR), Germany
[4]Department of Geography, University of Bonn, Germany
[5]Department of Civil and Environmental Engineering, National University of Singapore, Singapore
[6]Future Cities Laboratory, Singapore-ETH Centre, Singapore

Correspondence to: Yue Zhu (yue.zhu@sec.ethz.ch)

Abstract. Due to the limited availability of high-resolution topographic data, accurate flood simulation remains a significant challenge in many flood-prone regions, particularly in developing countries and in urban domains. While publicly available Digital Elevation Model (DEM) datasets are increasingly accessible, their spatial resolution is often insufficient for reflecting fine-scaled elevation details, which hinders the ability to simulate effectively pluvial floods in built environments. To address this issue, we implemented a deep learning-based method, which efficiently enhances the spatial resolution of DEM data, and quantified the improvement in flood simulation. The method employs a tailored multi-source input module, enabling it to effectively integrate and learn from diverse data sources. By utilizing publicly open global datasets, low-resolution DEM datasets (such as the 30m SRTM) in conjunction with high-resolution multispectral imagery (e.g., Sentinel-2A), our approach allows to produce a super-resolution DEM, which exhibits superior performance compared to conventional methods in reconstructing 10m DEM data based on 30m DEM data and 10m multispectral satellite images. Such superior performance translates, when applied to pluvial flood simulations, into significantly improved accuracy of floodwater depth and inundation area predictions compared to existing alternatives. This study underscores the practical value of machine-learning techniques that leverage publicly available global datasets to generate DEMs that allow enhancing flood simulations.

1 Introduction

The occurrence of severe floods has increased significantly due to climate change, which intensifies extreme rainfall events (Tabari, 2020). To address these challenges, high-resolution flood modelling is essential for making informed flood management decisions (Y. Wang et al., 2018). As one of the key inputs for flood simulations, accurate Digital Elevation Model (DEM) supports reliable flood simulation, in turn enabling the assessment of various flood mitigation strategies. However, the fidelity of flood simulations is heavily contingent upon the spatial resolution of DEM data (Hawker et al., 2018). At present, open datasets of DEM data with global coverage are predominantly available at raster resolutions coarser than 30×30 meters,

https://doi.org/10.5194/nhess-2024-207
Preprint. Discussion started: 18 November 2024


Natural Hazards and Earth System Sciences Discussions

failing to capture the fine-resolution local topography details that are crucial for flood modelling (Hawker et al., 2018). The lack of publicly open high-resolution DEM is particularly affecting data-scarce regions of the developing world, which are often the most vulnerable to the devastating impacts of floods (Malgwi et al., 2020). In response to these challenges, this research examines the effect of implementing a deep learning-based image super-solution model for generating high-resolution DEM data, and demonstrates the performance of the enhanced DEM data on improving pluvial flood simulations.

1.1 Existing methods for improving the spatial resolution of DEM

Improving the quality and spatial resolution of DEM data is in great demand in the fields of geospatial analysis and environmental modelling, as this can substantially improve the performance of a wide range of applications, particularly for natural hazard mapping, such as predicting floods (Tan et al., 2024), landslides (Brock et al., 2020), and volcanic flows (Deng et al., 2019). The most widely adopted approaches in existing studies of DEM super-resolution can be categorised into interpolation-based, data fusion-based, and learning-based methods (Zhou et al., 2023). The interpolation methods, such as bilinear and bicubic interpolations (Rees, 2000), are based on the concept of spatial autocorrelation, which posits that points in closer proximity are more alike than those that are more distant (Arun, 2013). While being straightforward and computationally efficient, their performance is often limited by the simplicity of terrain continuity and smoothness, potentially leading to over-smoothed terrain features (Yifan Zhang & Yu, 2022). Data fusion-based approaches leverage the unique strengths of different multi-source DEMs (Yue et al., 2015). During the fusion process of multiple DEM sources, height error maps or weight maps were commonly adopted for determining the importance of each DEM source. However, these simple methods may wrongly alter height values and cannot adequately resolve edge effects (Okolie & Smit, 2022).

Deep learning methods have significantly advanced the field of Single Image Super-Resolution (SISR), achieving superior performance in reconstructing high-resolution images from their low-resolution counterparts (Yang et al., 2019). Thus, besides interpolation-based and data fusion-based methods, deep learning-based super-resolution techniques have been implemented to enhance low-resolution DEM data (Demiray et al., 2021a, 2021b; Jiang et al., 2023; Kubade et al., 2020; Z. Li et al., 2023; Yue et al., 2015; Zhou et al., 2023, 2021, 2021). The implementations of deep learning-based SISR methods substantially improve the performance of remote sensing applications (Ling & Foody, 2019; Shang et al., 2022; Xie et al., 2022) and promote the utilisation of data that was previously underutilized due to limited spatial resolution (Zhu et al., 2021). For instance, Demiray et al. (2021a) employed Generative Adversarial Networks (GAN) for constructing a 3 feet high-resolution DEM from a 50 feet low-resolution DEM. Zhou et al. (2021) proposed a double filter deep residual neural network for DEM super-resolution. Demiray et al. (2021b) employed EfficientNetV2 as the backbone model to reconstruct DEMs up to 16 times finer than their initial spatial resolution. More recently, Li et al. (2023) developed a transformer-based deep learning network for upscaling DEM data with different upsampling factors (i.e., x2, x4). However, it should be noted that the majority of the deep learning applications in DEM super-resolution only employed low-resolution DEM data as input, without

https://doi.org/10.5194/nhess-2024-207
Preprint. Discussion started: 18 November 2024


Natural Hazards and Earth System Sciences Discussions

incorporating additional information. This can be insufficient to accurately capture the unique terrain features that characterize high-resolution DEM (Zhou et al., 2023) and that are required to support accurate flood modelling.

1.2 Multi-source deep learning for remote sensing applications

The increasing availability of data from diverse sensors has provided a practical basis for multi-source data analysis applications (Choi & Lee, 2019). The key benefits of integrating multi-source inputs include enhanced model performance through the combination of complementary data sources, and improved robustness and reliability of model performance in various remote sensing applications (J. Li et al., 2022). For instance, Shen *et al*. (2019) developed a deep learning-based model for drought monitoring, which employed multi-source remote sensing data as input, including DEM data, and meteorological and soil data. Lu et al. (2022) proposed a deep learning framework taking Google Earth imagery and point of interest heatmap as input data for urban functional zone extraction.

Many existing studies on DEM super-resolution tend to be solely based on a single source of low-resolution (LR) DEM input, which can be an ill-posed task as high-resolution details can hardly be accurately reconstructed without additional reference information (Yue et al., 2016). This also includes the attempts to include additional features generated from low-resolution DEM data. For instance, Zhang *et al*. (2023) calculated terrain gradient maps based on DEM data to guide the optimization process of a Convolutional Neural Network (CNN)-based DEM super-resolution. Zhou et al. (2023) proposed a terrain feature-based CNN for DEM super-resolution, which extracts slope and aspect from low-resolution DEM data and deploys them as additional features for model inputs and loss function. Although the additional low-resolution features facilitate performance gains in DEM super-resolution model training, they are constrained by an inherent lack of high-frequency details.

Arguably, an effective method to enhance DEM resolution could be that of fusing different data sources, such as integrating spatial data from higher-resolution sources (e.g., optical images), which offer more details related to terrain features, rather than directly upscaling low-resolution DEM (Tan et al., 2024), thereby offering great potential to improve the performance of learning-based DEM super-resolution. One example following this direction is found in Argudo et al. (2018), who examined the feasibility of combining natural colour aerial images and low-resolution DEM data as input to train a CNN for producing high-resolution DEM, suggesting improved performance compared with interpolation-based methods. Tan et al. (2024) introduced a deep learning-based DEM upscaling network that enhances low-resolution DEMs by predicting elevation differences using high-resolution optical images, and then fusing these predictions with the original DEM data through additional convolutional layers. It should be noted that these studies mainly employed natural colour images for feature fusion. In contrast, multispectral images can provide further features from non-visible wavelengths, such as near-infrared, allowing for more detailed and specialized analysis. This is supported by Chen *et al.* (2013), showcasing the effects of utilizing multispectral bands of satellite images on improving the performance of an interpolation-based DEM densification method.

https://doi.org/10.5194/nhess-2024-207
Preprint. Discussion started: 18 November 2024


Natural Hazards and Earth System Sciences Discussions

1.2 Significance of this study

In this literature context, this study aims to investigate the effectiveness of improving flood simulations using an enhanced DEM super-resolution generating method, which incorporates multispectral images, including the near-infrared band, as additional input for a deep learning-based DEM super-resolution model. Specifically, we provide the following main contributions: (i) the development of an efficient DEM super-resolution method that incorporates a tailored input module for processing multi-source and multi-scale input data, including both low-resolution DEM data and high-resolution multispectral satellite images; (ii) the use for this purpose of publicly open datasets, which ensures the generalizability of the method, especially for DEM-related applications in data-scarce regions; (iii) the quantitative assessment of the performance of the generated super-resolution DEM maps in improving pluvial flood simulations. The latter is achieved by evaluating the flood inundation maps generated based on different DEM super-resolution methods in terms of both floodwater depth and inundation area. Overall, this study represents a methodological advancement that showcases the practical value of multi-sourced deep learning-based methods for enhancing pluvial flood simulations, thus offering an exemplary pathway to address the issue of lacking high-resolution DEM for reliable risk assessments in the context of land use planning and disaster management.

2 Methodology

2.1 Residual Channel Attention Network (RCAN)

The proposed DEM super-resolution method employs the Residual Channel Attention Network (RCAN) as the backbone structure, which is a widely recognised method for single-image super-resolution (Y.Zhang et al., 2018). One of the key features employed in an RCAN is a deep residual network structure that integrates residual in residual (RIR) blocks. The RIR block combines long and short skip connections, enabling the network to learn more high-dimensional features from low-resolution to high-resolution images with a very deep structure, meanwhile avoiding the issue of vanishing gradient during training processes. Another key feature of RCAN is its use of channel attention mechanisms within each residual block. The channel attention mechanism weighs the importance of each channel, thus allowing RCAN to adaptively emphasise features from more important channels while suppressing less useful ones, thereby optimising reconstruction performance by focusing on the most significant features. This channel-attention mechanism can be particularly useful for processing multi-source input data (X. Liu et al., 2021). By integrating the RIR structure with channel-attention mechanisms, RCAN can extract and exploit hierarchical features from the input image effectively. However, since RCAN is developed for image super-resolution tasks on natural colour images, the structure of the model may need modification when handling inputs from different sources.

https://doi.org/10.5194/nhess-2024-207
Preprint. Discussion started: 18 November 2024

Natural Hazards and Earth System Sciences
Discussions

2.2 Multi-source and multi-scale input data fusion

By using RCAN as the backbone structure, this study proposes a multi-source method for DEM super-resolution, which incorporates high-resolution multispectral satellite images with low-resolution DEM data as the input to reconstruct high-resolution DEM data. Multispectral satellite images contain information captured across various spectral bands, including both visible light and invisible bands, which offer a wealth of information about surface materials, vegetation coverage, water bodies, and other landscape features (Carrão et al., 2008). Given the rich information and the open accessibility of high-resolution multispectral images, there is great potential to leverage the high-resolution spectral features from multispectral satellite images to compensate for the coarse information in low-resolution DEM and facilitate the reconstruction of high-resolution information on topography. It is anticipated that, by combining multispectral imagery with elevation data, deep learning models can access a more comprehensive set of features for prediction.

Given that two types of input data have different sizes, a tailored multi-source input block is integrated into the model structure before the first layer of the RCAN backbone structure (Fig. 1). In particular, the 30m DEM data is fed into a 2D convolutional layer with a kernel size of 3x3, a stride of 1, and padding size of 1. Meanwhile, the 10m multispectral satellite images are passed to another 2D convolutional layer that has a kernel size of 3x3 but with a stride of 3, which can effectively reduce the spatial dimensions of the input by a factor of 3. A Rectified Linear Unit (ReLU) activation function follows the convolution, introducing non-linearity and enhancing feature representation. As such, the information in 4-band multispectral input is encoded to a 4-channel tensor that has the same size as the encoded low-resolution data flow. Upon the same size of the two data flows, they can be concatenated along the channel dimension,

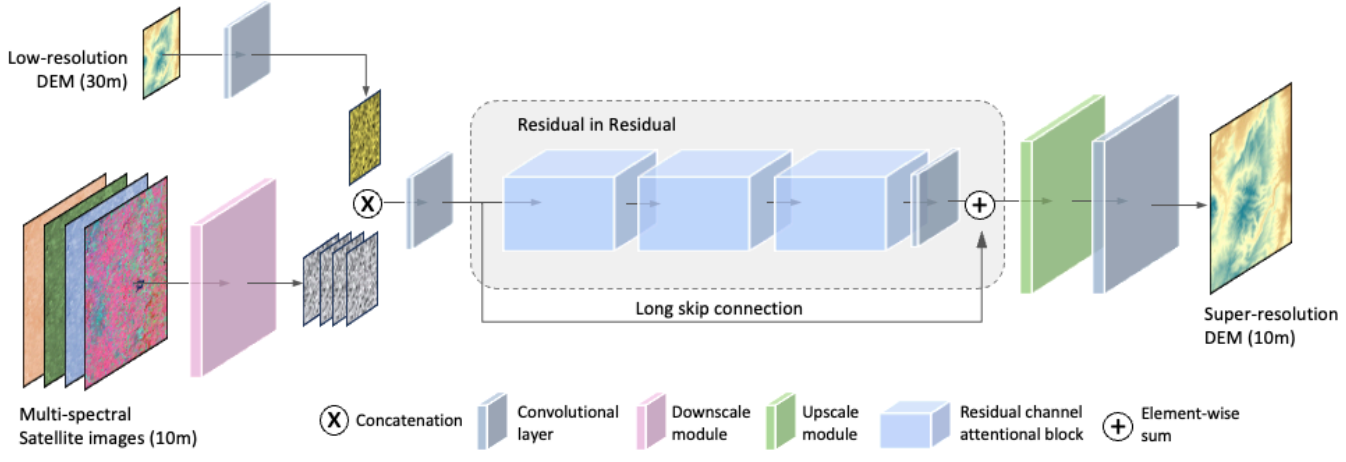

Fig. 1 The structure of the proposed DEM Super-resolution model, MS-RCAN. Low-resolution DEM data and 4-band multispectral satellite images are adopted as the input to reconstruct high-resolution DEM data.

https://doi.org/10.5194/nhess-2024-207
Preprint. Discussion started: 18 November 2024

Natural Hazards and Earth System Sciences
Discussions

and then processed by another 2D convolutional layer for data fusion of spatial and spectral information from multi-source inputs. The Mean Absolute Error (MAE) is adopted as the loss function. The proposed method is named RCAN-Multispectral (RCAN-MS) and is tested with two datasets at different geographical locations by comparing it with a series of baseline models in the following sections.

3 Experiment settings

3.1 Datasets

Although publicly open DEM datasets with global coverage have limited spatial resolution (coarser than 30m), the spatial resolution of publicly open multispectral satellite imagery with global coverage can reach 10m spatial resolution, such as Sentinel-2A, which has great potential to provide fine-grained features adding complementary information for DEM super-resolution. Thus, by employing the RCAN as the backbone model, this study proposes a novel method that utilises 10m multispectral satellite images and 30m DEM data to produce 10m super-resolution DEM data. Thus, considering the availability of datasets and the generalizability as global scales, we chose to work with a scale factor of ×3 for testing

Table 1. Information on the DEM data and multispectral satellite images in two datasets for the tests of DEM Super-resolution models

		Dataset I. England area	**Dataset II. Shenzhen & Hong Kong**
10m DEM	Collection source	LIDAR Composite DTM 2019 (Published by UK Environment Agency)	TanDEM-X (Provided by German Aerospace Centre (DLR))
	Spatial resolution	Resampled from 2m to 10m resolution	Resampled from 12m to 10m resolution
	Acquisition time	2019-09-01	2016-01-13
30m DEM	Collection source	Shuttle Radar Topography Mission (SRTM)	Shuttle Radar Topography Mission (SRTM)
	Spatial resolution	1 arc-second (~ 30m) resolution	1 arc-second (~ 30m) resolution
	Acquisition time	2014-09-23	2014-09-23
10m Multispectral Images	Collection source	Sentinel-2A	Sentinel-2A
	Spatial resolution	10m resolution	10m resolution
	Bands	Band 2 – Blue, Band 3 – Green, Band 4 – Red, Band 8 - Near-infrared	Band 2 – Blue, Band 3 – Green, Band 4 – Red, Band 8 - Near-infrared
	Acquisition time	2022-11-25 / 2023-01-21/ 2023-02-13	2023-12-25

https://doi.org/10.5194/nhess-2024-207
Preprint. Discussion started: 18 November 2024

Natural Hazards and Earth System Sciences
Discussions

DEM super-resolution models, which is also a scale factor widely adopted in most of the existing studies on image super-
155 resolution (P. Wang, Bayram, & Sertel, 2022).

Two datasets at different geographical locations were employed in this study for training and evaluation of DEM super-resolution methods, as well as for the simulation of pluvial floodwater distribution. All the data in these two datasets are collected from publicly open sources that have been widely adopted for remote sensing applications in urban environments, including SRTM (Wu, et al., 2019), TanDEM-X (Geiß et al., 2015), and Sentinel-2A (C. Li, et al., 2021).
160 The two datasets cover the areas of (i) England, UK (Dataset I), and (ii) Shenzhen and Hong Kong, China (Dataset II). Each dataset contains three different data sources (Table 1), including a 10m high-resolution DEM map, a 30m low-resolution DEM map, and the corresponding 10m multispectral satellite image composed of four bands (i.e., red, blue, green, near-infrared). It should be noted that, although the spatial resolution of the high-resolution DEM data in both datasets was pre-processed at the same resolution of 10m, they were collected from different sources due to data

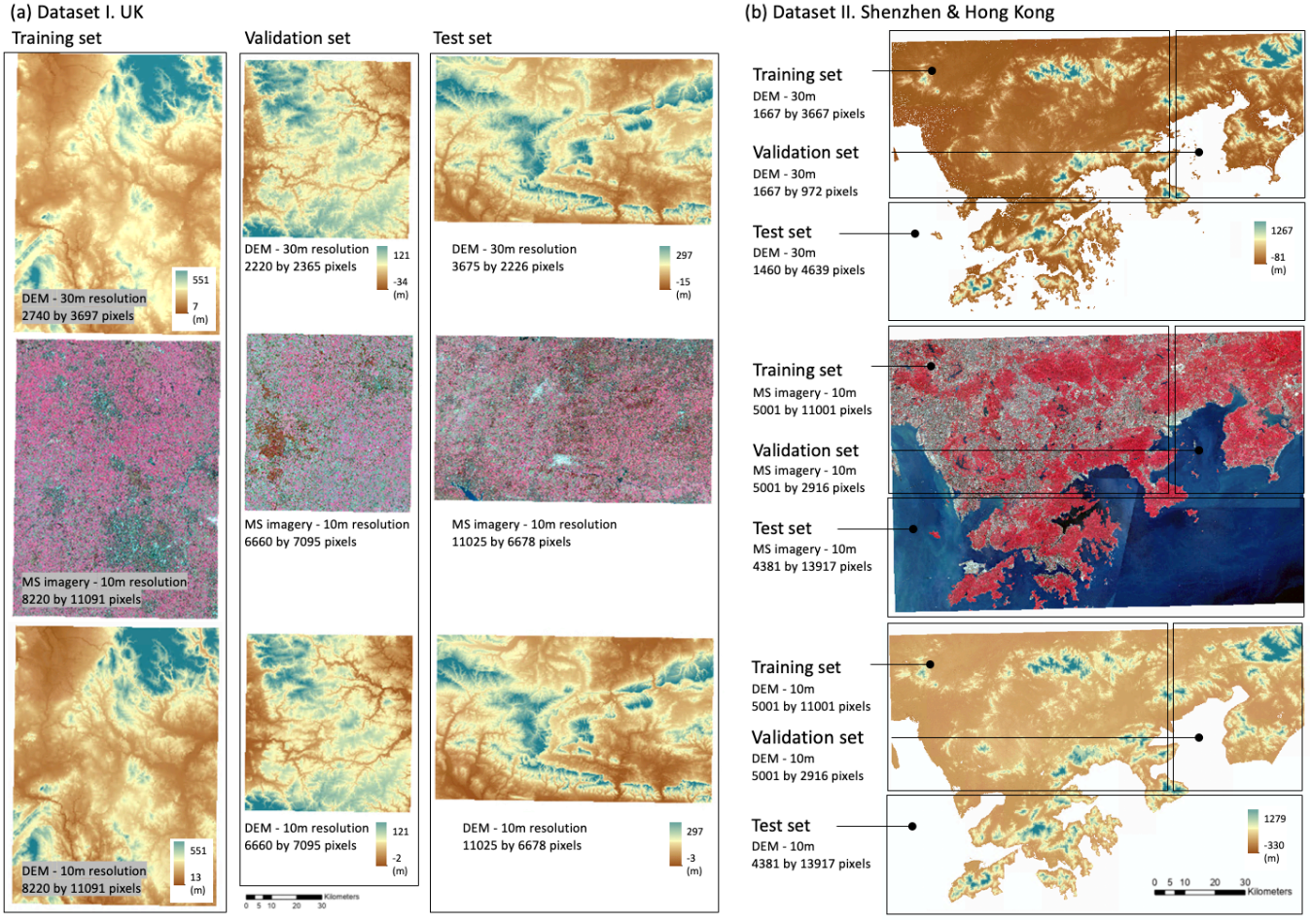

Fig. 2 Overview of the two datasets for DEM Super-resolution. (a) the training, validation, and test sets of Data set I. (b) the training, validation, and test sets of Data set II.

https://doi.org/10.5194/nhess-2024-207
Preprint. Discussion started: 18 November 2024

Natural Hazards and Earth System Sciences
Discussions

availability. However, such differences in data sources can also be leveraged to test the robustness and generalizability of the proposed methods.

As shown in Fig. 2, each dataset for the test on DEM super-resolution methods was split into three subsets, which are the training set, validation set, and test set. There are no spatial overlapping areas between the three subsets in each dataset. In each dataset, the three subsets were randomly subsampled into 2000, 200, and 300 small patches for training, validation, and testing, respectively. The size of the subsampled low-resolution DEM patches is 80×80 pixels, and the sizes of the subsampled high-resolution DEM and multispectral images are 240×240 pixels. Correspondingly, the DEM super-resolution models are trained with a target of upscaling the DEM data to three times its original size.

3.2 Experiment setup

The experiments were composed of two main stages (Fig. 3): (i) DEM super-resolution, and (ii) pluvial flood simulation. The first stage was centred on assessing the performance of DEM Super-resolution methods in enhancing the resolution of the original DEM data, whereas the second stage was to examine the effects of adopting the super-resolution DEM for pluvial flood simulations.

In the first stage, besides using the original high-resolution DEM data for performance evaluation, four additional baseline methods were employed for comparison with the performance of the proposed method, RCAN-MS. These baseline methods include a conventional bicubic interpolation method, and three other widely adopted neural network-based SISR methods, which are Super-resolution Convolutional Neural Network (SRCNN, Dong et al., 2016), Very Deep Convolutional Network (VDSR, Kim et al., 2016), and Residual Channel Attention Network (RCAN, Y.Zhang et al., 2018).

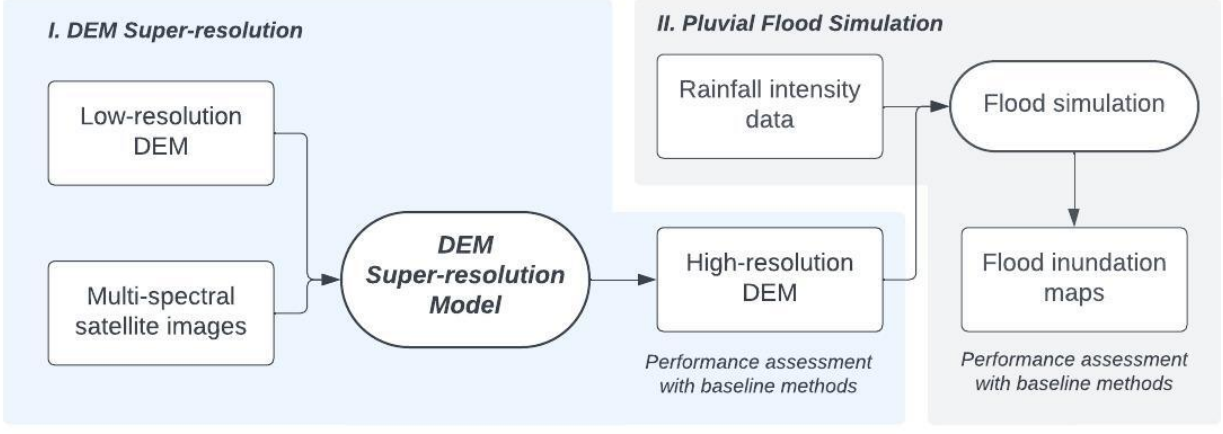

Fig. 3. Workflow of the experiments, including (i) establishing a DEM Super-resolution model to reconstruct a high-resolution DEM, then (ii) adopting the high-resolution DEM for pluvial flood simulations.

https://doi.org/10.5194/nhess-2024-207
Preprint. Discussion started: 18 November 2024


Natural Hazards and Earth System Sciences
Discussions

The training of DEM Super-resolution models was conducted with two RTX 4090 GPUs on High-performance computing (HPC) clusters. All the test methods were trained with a batch size of 8 and a learning rate of 8*10-5. Regarding the stopping criteria for mode performance evaluation, all the models were trained for 200 epochs with the data in the training set, after which the epoch yielding the smallest MAE values on the validation set was selected for further performance elevation. In particular, the assessments of model performance were conducted on the test set, which was neither involved in the training process nor in the stopping criteria. The Mean Absolute Error (MAE), Mean Square Error (MSE), Peak Signal-to-Noise Ratio (PSNR) and Structural Similarity Index Measure (SSIM) were employed to evaluate the performance of DEM super-resolution models. PSNR and SSIM are two widely used evaluation metrics in image super-resolution tasks (Dong et al., 2016; Kim et al., 2016; Yang et al., 2019). The PSNR measures the quality of reconstruction of a lossy transformation (e.g., image compression) (Z. Wang et al., 2021), with higher values indicating a smaller difference. The SSIM measures the similarity between two images, specifically targeting changes in brightness, contrast, and structure (Z. Wang et al., 2021).

For both the UK and China datasets, the DEM data generated by all the downscaling methods in the super-resolution test were adopted as input for flood simulation. In each dataset, a subarea of 450 by 600 pixels was cropped for pluvial flood simulation. The simulation is conducted using a cellular automata model, Caddies (Guidolin et al., 2016), which is known for efficient pluvial flood simulation in urban environments (Liu, et al., 2018; Y. Wang, et al., 2019; Y. Wang et al., 2023).

The pluvial flood simulation was based on a 100-year return period, and 30-minute duration rainfall as a forcing scenario. Since the two geographical locations feature different climate conditions, the rainfall intensity corresponding to the 100-year return period rainfall was set based on the Intensity-duration-frequency (IDF) curves of the UK and Hong Kong, respectively. The IDF curve of the UK is computed using the hourly rainfall data recorded at the rain gauge station of Seathwaite, North England, and downloaded from the MIDAS UK sub-hourly rainfall observations dataset (Met Office, 2006). The adopted IDF curve for Hong Kong is according to a report published by the Civil Engineering and Development Department, the Government of the Hong Kong Special Administrative Region (Tang & Cheung, 2011). Specifically, the 100-year return period rainfall intensity for a 30-minute duration is 42 mm/h for Dataset I, and 190 mm/h for Dataset II. The simulated flood maps were evaluated by comparing their similarity with the flood map generated based on reference high-resolution DEM data. Both flood depth values and flood area coverage were assessed. The evaluation metrics to measure flood depth values are MAE and MSE, and the metric for evaluating the flood areas is Intersection over Union (IoU), which is a widely adopted method to assess the accuracy of a predicted area in comparison to the target area found in ground truth data (Rahman & Wang, 2016).

https://doi.org/10.5194/nhess-2024-207
Preprint. Discussion started: 18 November 2024

Natural Hazards and Earth System Sciences
Discussions

4 Experiment settings

4.1 DEM Super-resolution

The experimental results of the comparison between the proposed DEM super-resolution method and all the baseline methods are presented in Table 2, including the comparisons in both datasets. For Dataset I, the RCAN-MS method demonstrates a marked improvement over the Bicubic method, reducing the MAE from 3.01 to 2.20, and the MSE from 19.02 to 8.71. This enhancement is also reflected in the values of PSNR and SSIM, which increase from 33.41 to 36.76, and from 0.46 to 0.62, respectively, suggesting a substantially improved fit to the target high-resolution DEM. Similarly, Dataset II results reveal that RCAN-MS significantly outperforms the bicubic interpolation method, with the MAE sharply decreasing from 9.976 to 5.918, and the MSE from 186.035 to 67.588. The RCAN method, serving as the backbone method for RCAN-MS, shows better results than the other deep learning-based methods such as SRCNN and VDSR across both datasets, underscoring the superior performance of the RCAN-based architecture in the task of DEM super-solution. Specifically, for Dataset I, RCAN posts an MAE of 2.60 and an MSE of 12.95, with a PNSR of 35.05 and an SSIM of 0.60, which are better than those for SRCNN and VDSR. In Dataset II, RCAN achieves an MAE of 6.41 and an MSE of 83.53, with a PNSR of 38.40 and an SSIM of 0.68, further confirming its robustness. The performance superiority of the proposed RCAN-MS method is evident across all metrics in both datasets, demonstrating its enhanced capability in generating high-fidelity super-resolution DEM data. This is exemplified by the significant reductions in MAE and MSE and the corresponding increase in PNSR and SSIM values, signifying its substantial improvements over the baseline methods.

Fig. 4 and Fig. 5 present the two selected patches from the test sets of Datasets I and II for visual assessment of the performance of the super-resolution DEM maps, in which a subarea of exemplary patches is additionally enlarged

Table 2. Evaluation results of all the tested methods on two test sets with different geographical locations

	Test set of Dataset I.				*Test set of Dataset II.*			
	MAE	**MSE**	**PNSR**	**SSIM**	**MAE**	**MSE**	**PNSR**	**SSIM**
bicubic	3.0078	19.0206	33.4055	0.4621	9.2924	163.0170	35.4505	0.6091
SRCNN	2.7665	15.5027	34.2901	0.5776	6.8153	94.1950	37.8500	0.6794
VDSR	2.6530	13.4866	34.8653	0.5737	6.6412	88.7638	38.1110	0.6811
RCAN	2.5967	12.9453	35.0460	0.5975	6.4150	83.5288	38.3950	0.6838
RCAN-MS	**2.1952**	**8.7102**	**36.7605**	**0.6205**	**5.8181**	**66.6251**	**39.3543**	**0.7411**

https://doi.org/10.5194/nhess-2024-207
Preprint. Discussion started: 18 November 2024

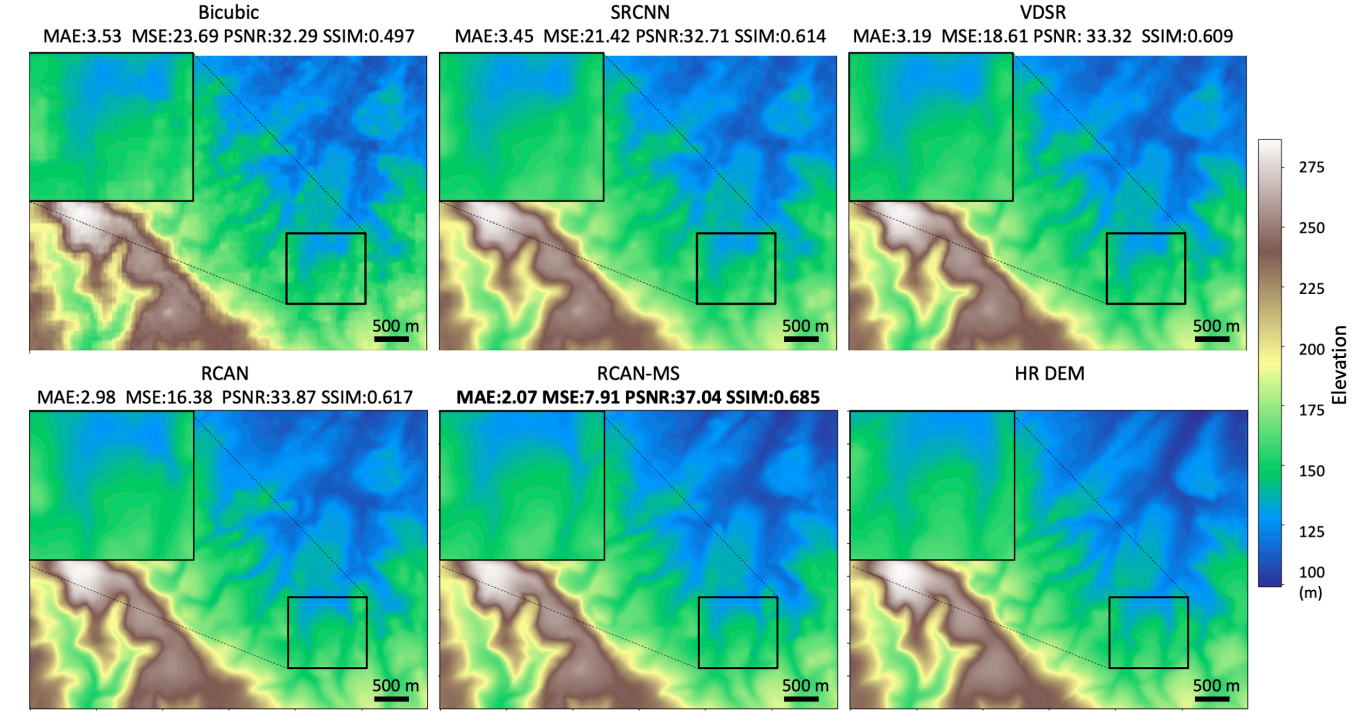

Fig. 4 Comparison of DEM maps in the test set of Dataset I. generated by the proposed method, RCAN-MS, other baseline methods and the original high-resolution DEM map in Dataset I.

for further visual comparison of details. These two exemplary patches of the test sets are employed for pluvial flood simulation in the following section. The performance related to using the super-resolution DEM maps produced by all the tested methods was compared with that of the corresponding reference high-resolution DEM map. The values of the evaluation metrics (i.e., MAE, MSR, PSNR, SSIM) are also summarised in the two figures. The ranking of the performance of all the tested methods is aligned with the overall evaluation of the test sets reported in Table 2. For the exemplary patch from Dataset I, bicubic interpolation exhibits an MAE of 3.53 and an MSE of 23.69, with a PNSR of 32.29 and an SSIM of 0.497. RCAN offers a larger magnitude of enhancement than SRCNN and VDSR with an MAE of 2.98 and an MSE of 16.38, with a PNSR of 33.87 and an SSIM of 0.617, demonstrating a notable increase in precision. RCAN-MS stands out among all the tested methods, recording the lowest MAE of 2.07 and an MSE of 7.91, while also achieving the highest PSNR of 37.04 and the highest SSIM of 0.685.

The enlarged area of Dataset II is situated at a relatively higher elevation in the patch (Fig. 5). Despite the different geographical locations of the exemplary patches in the two datasets, the results of the DEM super-resolution test on Dataset II align with the results of Dataset I. RCAN method surpasses SRCNN and VDSR with an MAE of 5.70 and an MSE of 57.38, coupled with a PNSR of 39.91 and an SSIM of 0.685. The proposed method RCAN-MS also presents in the case of Dataset II the best performance among the methods tested, with the lowest error metrics with an MAE of

https://doi.org/10.5194/nhess-2024-207
Preprint. Discussion started: 18 November 2024

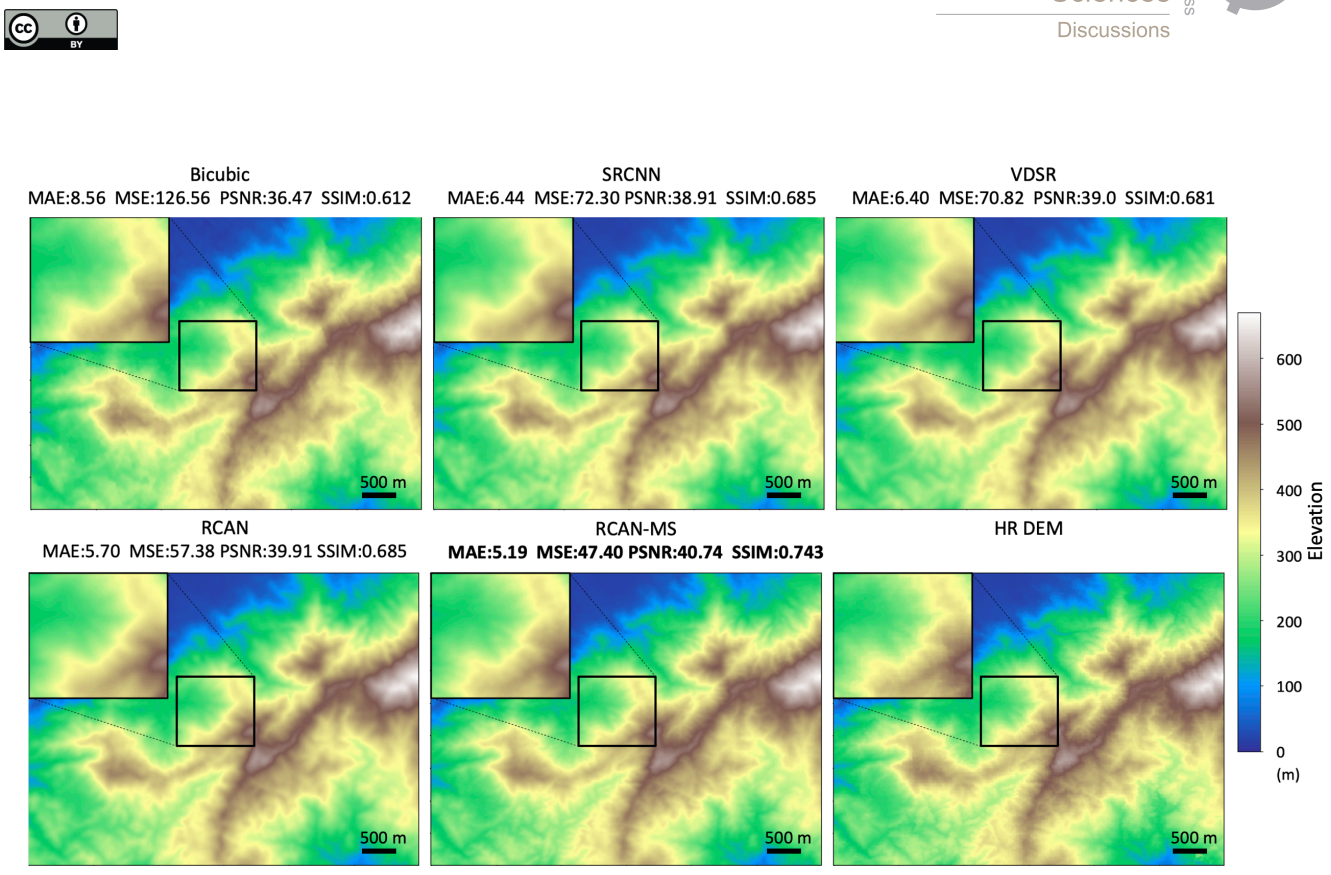

Fig. 5. Comparison of DEM maps in the test set of Dataset II generated by the proposed method, RCAN-MS, other baseline methods and the original high-resolution DEM map.

5.19 and an MSE of 47.40, and the highest values in PNSR (40.74) and SSIM (0.743), highlighting its effectiveness in reconstructing fine-grained information and also capturing the complexity of terrain elevations.

Arguably, in contrast to the exemplary patch from Dataset II (Fig. 5), the patch from Dataset I is characterized by a relatively flatter terrain (Fig. 4). it is noteworthy that flatter areas could pose a greater challenge due to smaller variations in elevation, which are closer in magnitude to the vertical accuracy of the DEM, potentially increasing the likelihood of error. Thus, demonstrating the effectiveness of RCAN-MS in such conditions, as seen with Dataset I, manifestly provides a more stringent test of its capabilities in maintaining accuracy across subtler elevation changes.

The conventional image interpolation method, bicubic, presents the worst performance in the exemplary patches from both Dataset I and Dataset II with pixelated DEM maps that lack fine-grained features. Regarding the deep-learning-based super-resolution methods in Dataset I (Fig. 4), the super-resolution DEM images generated by SRCNN and VDSR exhibit over-smoothing effects which lead to a loss of details. In contrast, the super-resolution DEM images produced by RCAN and RCAN-MS presented substantially less blurring effect than other baseline methods. Furthermore, by incorporating multispectral satellite images as part of the input, RCAN-MS generated a super-resolution DEM image with finer details in elevation difference compared with RCAN, which showed the best performance among all the baseline methods.

https://doi.org/10.5194/nhess-2024-207
Preprint. Discussion started: 18 November 2024

Natural Hazards and Earth System Sciences
Discussions

To assess the extent to which the improved DEM data can facilitate pluvial flood simulation, the exemplary patches of the two test sets were adopted as the input data in the next stage experiment for pluvial flood simulation.

4.2 Pluvial flood simulation

Pluvial flood simulations were conducted using the super-resolution DEM data of the two exemplary patches presented in Fig. 4 and Fig. 5, including the DEM data produced by all the tested methods. As mentioned further above, the rainfall scenario for pluvial flood simulation was set to be a 30-minute duration for a 100-year return period for both datasets, with intensities set according to the geographical location, respectively 42 mm/h for England in Dataset I and 190 mm/h for Hong Kong in Dataset II.

Fig. 6 demonstrates the simulated pluvial floodwater inundation maps using super-resolution DEM maps of the exemplary patch of Dataset I, which are illustrated in Fig. 4. Comparing the various flood inundation maps in Fig. 6, it can be observed that the flood inundation map generated based on RCAN-MS replicates more similarity of floodwater distribution obtained from using the high-resolution DEM, compared to the other super-resolution generating methods considered (i.e., Bicubic, SRCNN, VDSR, RCAN), thus reflecting the effects of less elevation errors of DEM data in flood simulation. This can be particularly observed in the enlarged areas in Fig. 6, the inundated area predicted based on

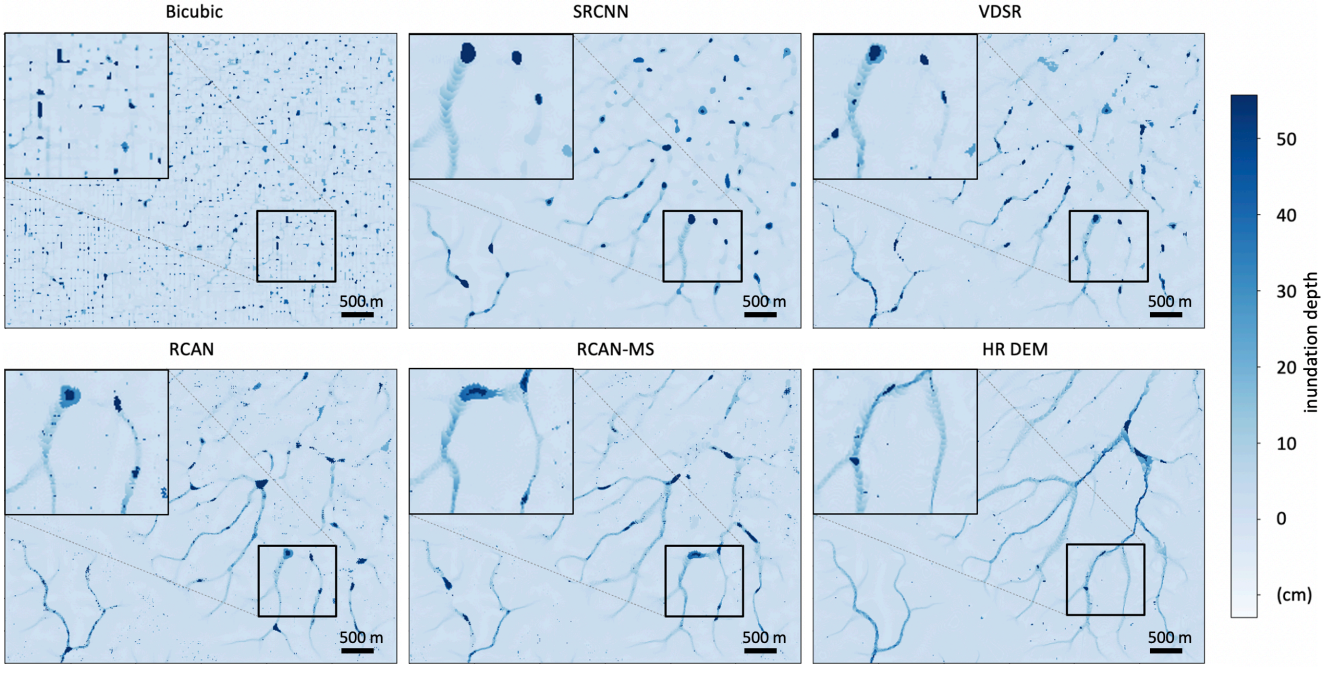

Fig. 6 Maps of pluvial flood inundation depth were simulated using super-resolution DEM data and compared with the original high-resolution DEM data in an exemplary patch of Dataset I.

https://doi.org/10.5194/nhess-2024-207
Preprint. Discussion started: 18 November 2024

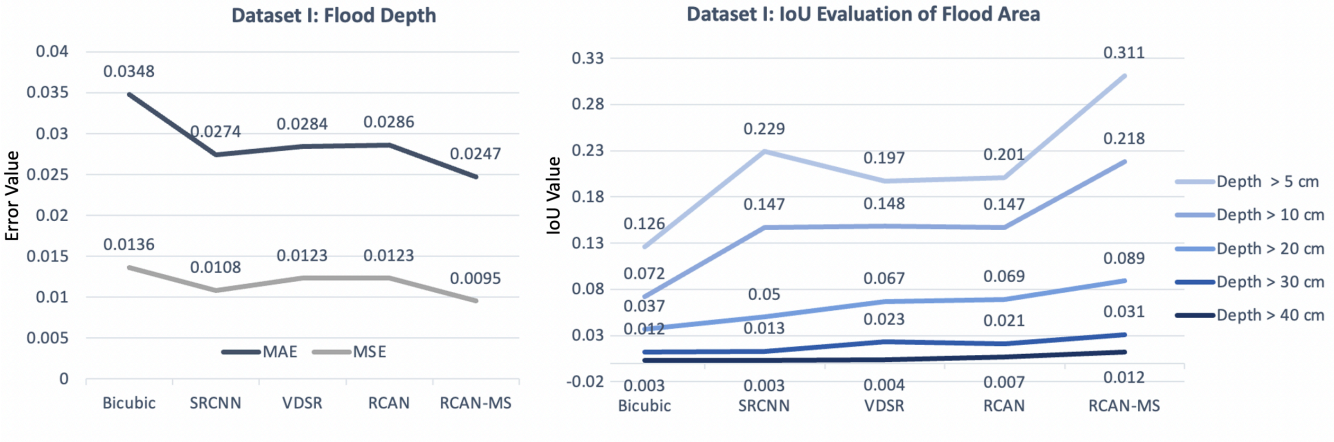

Fig. 7 Performance evaluation of pluvial flood simulations based on super-resolution DEM data compared with the original high-resolution DEM data in the exemplary patch of Dataset I. Left: MAE and MSE comparison of flood depth values; right: IoU evaluation of the spatial coverage of flood area delineated by different depth thresholds from 5cm to 40 cm.

the RCAN-MS method exhibits greater consistency with the high-resolution DEM, with the distribution of floodwater appearing more contiguous, while other methods display more abrupt changes in water levels which can be inferred from the scattered dark blue shading within the maps.

The performance in terms of floodwater depth and flood inundation area using super-resolution DEM data in the exemplary patch of Dataset I was also quantitively evaluated and compared with the values obtained from simulations that used the reference high-resolution DEMs (Fig. 7). The errors of floodwater depth were evaluated using MAE and MSE. The RCAN-MS method outperforms the other methods with the lowest MAE of 0.0247 and the lowest MSE of 0.0095, scoring an approximately 30% improvement compared with conventional bicubic methods in both MAE and MSE. The accuracy of flood areas, defined using varying thresholds (i.e., 5 cm, 10 cm, 20 cm, 30 cm, 40 cm), was assessed using Intersection over Union (IoU), which measures the overlapping areas between the predicted flood areas defined using these thresholds. Here, the RCAN-MS method generally shows higher IoU values at different depth thresholds compared to other methods, suggesting it is more precise in predicting the actual flood-affected area that will emerge from using the original DEM. Particularly for the flooded area with thresholds of 5 cm and 10 cm, the RCAN-MS method exhibits the highest IoU values with an improvement of 146% and 202% compared with bicubic interpolation.

The comparison of flood simulation results generated based on super-resolution DEM data from Dataset II are presented in Fig. 8 and Fig. 9. The visual inspection of flood inundation maps and quantitative evaluation suggest that results generally align with the performance obtained for Dataset I. In particular, the flood inundation map generated based on RCAN-MS shows more fine-resolution details matching the floodwater distribution generated with the reference high-resolution DEM. Furthermore, the RCAN-MS-based flood inundation map yields the smallest MAE

https://doi.org/10.5194/nhess-2024-207
Preprint. Discussion started: 18 November 2024

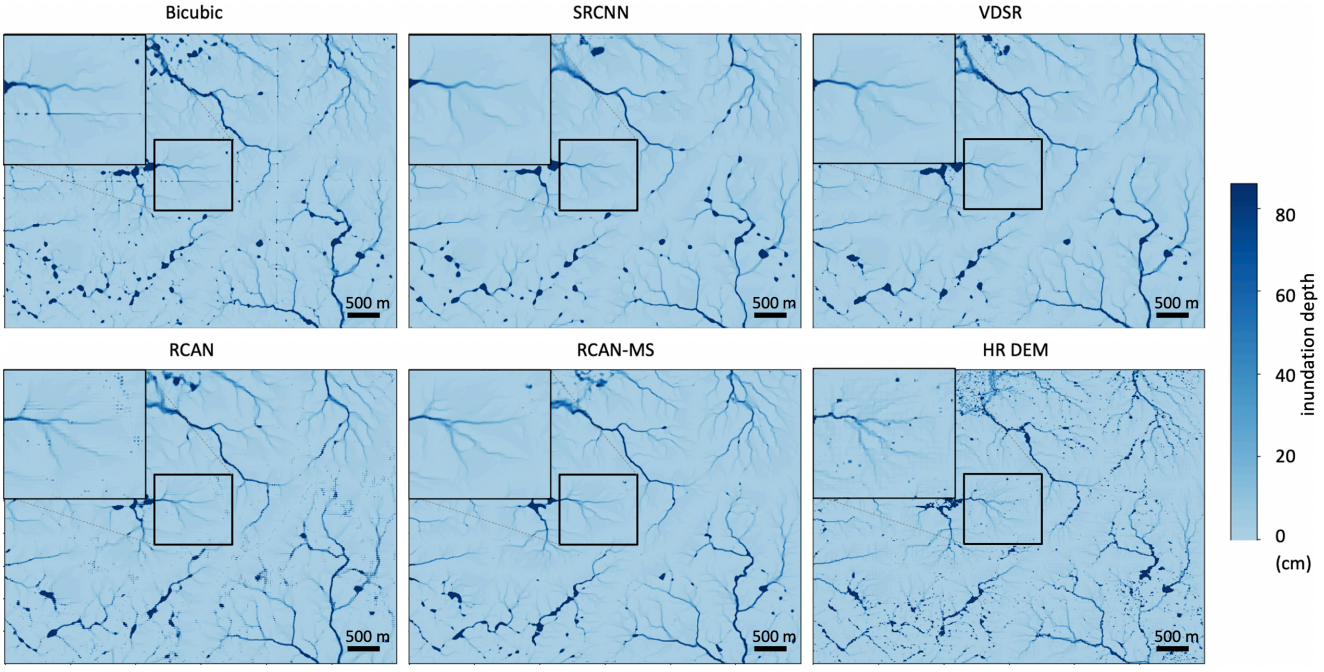

Fig. 8 Maps of pluvial flood inundation depth were simulated using super-resolution DEM data and compared with the original high-resolution DEM data in an exemplary patch of Dataset II.

(0.1193) and MSE values (0.3009), indicating approximately 13% and 15% improvement in flood depth errors compared with the bicubic-based flood inundation map.

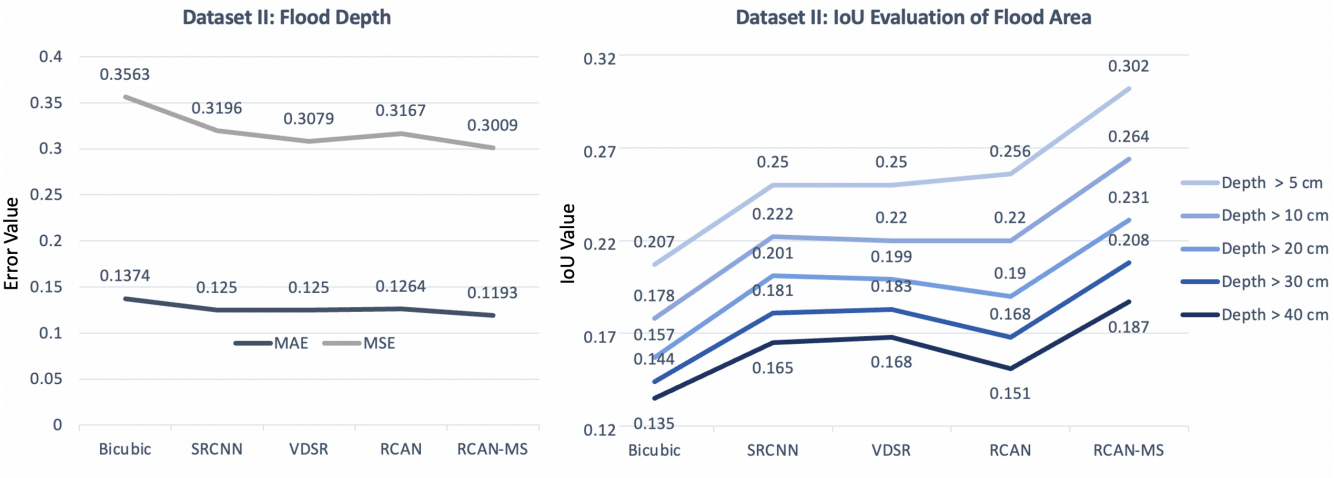

Fig. 9 Performance evaluation of flood simulation maps produced based on super-resolution DEM data compared with the original high-resolution DEM data in the exemplary patch of Dataset II. Left: MAE and MSE comparison of flood depth values; right: IoU evaluation of the spatial coverage of flood area delineated by different depth thresholds from 5cm to 40 cm.

https://doi.org/10.5194/nhess-2024-207
Preprint. Discussion started: 18 November 2024


Natural Hazards and Earth System Sciences
Discussions

5 Discussion

Among the investigated techniques to generate super-resolution DEMs, the here developed RCAN-MS provided superior performance compared to other baseline methods not only in terms of accuracy with respect to the high-resolution reference DEM, but also with respect to the impact that its use has on flood simulation. Such superior performance is due to learning from multi-source inputs, particularly the incorporation of high-resolution multispectral satellite images, enabling it to achieve fine-resolution details, while mitigating the pepper-and-salt noise effects in RCAN but avoiding over-smoothing in SRCNN and VDSR. Arguably, in RCAN-MS, the improvement effect of the multi-source input on DEM super-resolution is likely due to the additional feature extracted from multispectral information, which can facilitate the estimation of the reflectance of varying land cover types, and contribute to a better understanding of land cover features interact with different terrains, thus leading to more detailed and accurate terrain reconstructions (Chen et al., 2013). Specifically, the differentiation between vegetated areas and bare soil in multispectral data can increase the performance of model in accurately predicting elevation changes and surface contours. The variety of spectral bands helps in distinguishing between features that may have similar elevation profiles but different spectral characteristics, such as the different inter-class variations between urban areas and rocky terrain.

Most importantly, the RCAN-MS method to build a high-resolution DEM substantially enhances the accuracy of flood simulations by producing DEM data with sufficient spatial resolution and improved terrain reconstructions. It is important to note that in principle better performance in DEM super-resolution does not necessarily guarantee an improvement in flood simulation accuracy. This is evident in the experimental results that, although the backbone method RCAN achieved the second-best performance in the evaluation of DEM super-resolution tests in both datasets, RCAN fell short in pluvial flood simulation when compared to SRCNN and VDSR. This inferior performance can likely be attributed to the presence of pepper-and-salt noise within the flood inundation maps simulated from RCAN, where shallow-depth flooded pixels appear scattered. In contrast, SRCNN and VDSR, known for producing smoother ground surfaces, result in DEMs that lead to fewer instances of scattered floodwater pixels. Therefore, despite RCAN yielding fewer errors in DEM super-resolution compared to SRCNN and VDSR, the latter models achieve higher scores in simulated flood inundation maps due to the reduced occurrence of pepper-and-salt noise. This issue was substantially alleviated in the results of RCAN-MS due to the integration of multi-spectral satellite images. The integration of multi-spectral satellite imagery in the RCAN-MS method has proven to be effective in reducing noise and improving flood simulation accuracy. Incorporating additional data sources enables the model to better represent complex terrain features, which play crucial roles in flood simulation performance.

While the present study shows the significantly better-performing nature of the RCAN-MS technique compared to other well-established methods, one should note that the study is also characterised by some limitations. First, we

https://doi.org/10.5194/nhess-2024-207
Preprint. Discussion started: 18 November 2024


Natural Hazards and Earth System Sciences Discussions

tailored the model structure to take advantage of multi-scale and multi-source input data for DEM super-resolution, but only incorporated 4-band multispectral satellite images as additional features, other terrain-related features (e.g., slope, aspect) that may bring further improvement to model performance were not tested in this study. Second, for the two datasets tested in this study, as we intend to examine the performance of proposed models with a direct and efficient workflow, we did not apply data pre-processing techniques (e.g., noise reduction) on the high-resolution DEM data. There may still be room for improvement in flood simulations using super-resolution DEM data that have pre-processed high-resolution DEM as training targets. Finally, it should be acknowledged that variations in acquisition dates of data from diverse sources can lead to minor inconsistencies in datasets. These temporal discrepancies, especially between multispectral satellite imagery, and between low-resolution and high-resolution images, may affect the efficacy of DEM super-resolution generation, potentially reducing its performance.

In future works, further tests could focus on investigating the impact of including additional terrain-related features on model performance, as well as examine the performance of the proposed methods with different downscaling factors where higher resolution DEM data is available as training targets. Moreover, this study performed pluvial flood simulations using a cellular automata-based model forced with a rainfall scenario of a 1-in-100-year return period, further tests could assess the effects of super-resolution DEM with alternative rainfall scenarios, and other flood simulation models that involve further elements influencing the flooding, such surface permeability and drainage networks. In addition, this improvement also paves the way for potential applications on other types of hazard simulations that are sensitive to variations in DEM resolution and noise, such as landslides, tsunamis-derived floods, and volcanic flows.

6 Conclusion

This study addresses the critical challenge of accurate flood simulation in regions where high-resolution DEM data is limited. We developed and implemented a deep learning-based DEM super-resolution method, incorporating multi-source input data, including low-resolution DEM and high-resolution multispectral imagery. The experiment suggests that the enhanced multi-source DEM super-resolution method, RCAN-MS, significantly improves the accuracy of the DEM for the purpose of pluvial flood simulations, particularly in terms of floodwater depth and inundation area predictions. The integration of Sentinel-2A multispectral data with the 30m SRTM DEM allows for the reconstruction of 10m DEM data with higher fidelity compared to conventional methods. The superior performance of RCAN-MS in flood simulation compared to its backbone method also highlights the importance of incorporating additional data sources to improve terrain representation and reduce noise, thereby enhancing flood simulation accuracy.

By leveraging publicly available global datasets, this approach offers a promising solution for regions with limited access to high-resolution topographic data, enabling not only more precise flood simulations, but also the potential to

https://doi.org/10.5194/nhess-2024-207
Preprint. Discussion started: 18 November 2024

generate large-scale high-resolution DEMs from existing publicly available coarse DEMs and, thus, opens new possibilities for resilience development and resource allocation, potentially not only contributing to flood risk reduction, but also to broader applications in simulating other natural hazards, such as landslides, tsunamis, and volcanic flows, where accurate terrain representation is essential.

Code availability. Codes are available upon request from the corresponding author. The software for cellular automata-based pluvial flood simulation can be downloaded from the CADDIES website (https://www.exeter.ac.uk/research/centres/cws/resources/caddies/).

Data availability. Data collected and generated during the experiments are available upon request.

Author contributions. All authors contributed to the idea and scope of the paper. Yue Zhu contributed to conceptualization, data curation, formal analysis, methodology, data analysis, software and script, validation, and original draft writing. Paolo Burlando, Puay Yok Tan, and Simone Fatichi contributed to supervision, review and editing, and funding acquisition. Christian Geiß contributed to data acquisition and supervision.

Conflict of Interest. No conflict of interest amongst the authors.

Acknowledgements

This research was funded in part by the Future Cities Lab Global programme. Future Cities Lab Global is supported and funded by the National Research Foundation, Prime Minister's Office, Singapore under its Campus for Research Excellence and Technological Enterprise (CREATE) programme and ETH Zurich (ETHZ), with additional contributions from the National University of Singapore (NUS), Nanyang Technological University (NTU), and the Singapore University of Technology and Design (SUTD).

References

Argudo, O., Chica, A., & Andujar, C. (2018). Terrain Super-resolution through Aerial Imagery and Fully Convolutional Networks. *Computer Graphics Forum*, *37*(2), 101–110. doi: 10.1111/cgf.13345

Arun, P. V. (2013). A comparative analysis of different DEM interpolation methods. *The Egyptian Journal of Remote Sensing and Space Science*, *16*(2), 133–139. doi: 10.1016/j.ejrs.2013.09.001

https://doi.org/10.5194/nhess-2024-207
Preprint. Discussion started: 18 November 2024

Brock, J., Schratz, P., Petschko, H., Muenchow, J., Micu, M., & Brenning, A. (2020). The performance of landslide susceptibility models critically depends on the quality of digital elevation models. *Geomatics, Natural Hazards and Risk*, *11*(1), 1075–1092. doi: 10.1080/19475705.2020.1776403

Carrão, H., Gonçalves, P., & Caetano, M. (2008). Contribution of multispectral and multitemporal information from MODIS images to land cover classification. *Remote Sensing of Environment*, *112*(3), 986–997. doi: 10.1016/j.rse.2007.07.002

Chen, Z., Qin, Q., Lin, L., Liu, Q., & Zhan, W. (2013). DEM Densification Using Perspective Shape From Shading Through Multispectral Imagery. *IEEE Geoscience and Remote Sensing Letters*, *10*(1), 145–149. doi: 10.1109/LGRS.2012.2195471

Choi, J.-H., & Lee, J.-S. (2019). EmbraceNet: A robust deep learning architecture for multimodal classification. *Information Fusion*, *51*, 259–270. doi: 10.1016/j.inffus.2019.02.010

Demiray, B. Z., Sit, M., & Demir, I. (2021a). D-SRGAN: DEM Super-Resolution with Generative Adversarial Networks. *SN Computer Science*, *2*(1), 48. doi: 10.1007/s42979-020-00442-2

Demiray, B. Z., Sit, M., & Demir, I. (2021b, September 20). *DEM Super-Resolution with EfficientNetV2*. arXiv. doi: 10.48550/arXiv.2109.09661

Deng, F., Rodgers, M., Xie, S., Dixon, T. H., Charbonnier, S., Gallant, E. A., … Richardson, J. A. (2019). High-resolution DEM generation from spaceborne and terrestrial remote sensing data for improved volcano hazard assessment—A case study at Nevado del Ruiz, Colombia. *Remote Sensing of Environment*, *233*, 111348. doi: 10.1016/j.rse.2019.111348

Dong, C., Loy, C. C., He, K., & Tang, X. (2016). Image Super-Resolution Using Deep Convolutional Networks. *IEEE Transactions on Pattern Analysis and Machine Intelligence*, *38*(2), 295–307. doi: 10.1109/TPAMI.2015.2439281

Geiß, C., Wurm, M., Breunig, M., Felbier, A., & Taubenböck, H. (2015). Normalization of TanDEM-X DSM Data in Urban Environments With Morphological Filters. *IEEE Transactions on Geoscience and Remote Sensing*, *53*(8), 4348–4362. doi: 10.1109/TGRS.2015.2396195

Guidolin, M., Chen, A. S., Ghimire, B., Keedwell, E. C., Djordjević, S., & Savić, D. A. (2016). A weighted cellular automata 2D inundation model for rapid flood analysis. *Environmental Modelling & Software*, *84*, 378–394. doi: 10.1016/j.envsoft.2016.07.008

Hawker, L., Bates, P., Neal, J., & Rougier, J. (2018). Perspectives on Digital Elevation Model (DEM) Simulation for Flood Modeling in the Absence of a High-Accuracy Open Access Global DEM. *Frontiers in Earth Science*, *6*. Retrieved from https://www.frontiersin.org/articles/10.3389/feart.2018.00233

Jiang, Y., Xiong, L., Huang, X., Li, S., & Shen, W. (2023). Super-resolution for terrain modeling using deep learning in high mountain Asia. *International Journal of Applied Earth Observation and Geoinformation*, *118*, 103296. doi: 10.1016/j.jag.2023.103296

Kim, J., Lee, J. K., & Lee, K. M. (2016). Accurate Image Super-Resolution Using Very Deep Convolutional Networks. *2016 IEEE Conference on Computer Vision and Pattern Recognition (CVPR)*, 1646–1654. doi: 10.1109/CVPR.2016.182

https://doi.org/10.5194/nhess-2024-207
Preprint. Discussion started: 18 November 2024

Kubade, A. A., Sharma, A., & Rajan, K. S. (2020). Feedback Neural Network Based Super-Resolution of DEM for Generating High Fidelity Features. *IGARSS 2020 - 2020 IEEE International Geoscience and Remote Sensing Symposium*, 1671–1674. doi: 10.1109/IGARSS39084.2020.9323310

Li, C., Shao, Z., Zhang, L., Huang, X., & Zhang, M. (2021). A Comparative Analysis of Index-Based Methods for Impervious Surface Mapping Using Multiseasonal Sentinel-2 Satellite Data. *IEEE Journal of Selected Topics in Applied Earth Observations and Remote Sensing*, *14*, 3682–3694. doi: 10.1109/JSTARS.2021.3067325

Li, J., Hong, D., Gao, L., Yao, J., Zheng, K., Zhang, B., & Chanussot, J. (2022). Deep learning in multimodal remote sensing data fusion: A comprehensive review. *International Journal of Applied Earth Observation and Geoinformation*, *112*, 102926. doi: 10.1016/j.jag.2022.102926

Li, Z., Zhu, X., Yao, S., Yue, Y., García-Fernández, Á. F., Lim, E. G., & Levers, A. (2023). A large scale Digital Elevation Model super-resolution Transformer. *International Journal of Applied Earth Observation and Geoinformation*, *124*, 103496. doi: 10.1016/j.jag.2023.103496

Ling, F., & Foody, G. M. (2019). Super-resolution land cover mapping by deep learning. *Remote Sensing Letters*, *10*(6), 598–606. doi: 10.1080/2150704X.2019.1587196

Liu, H., Wang, Y., Zhang, C., Chen, A. S., & Fu, G. (2018). Assessing real options in urban surface water flood risk management under climate change. *Natural Hazards*, *94*(1), 1–18. doi: 10.1007/s11069-018-3349-1

Liu, X., Jiao, L., Li, L., Tang, X., & Guo, Y. (2021). Deep multi-level fusion network for multi-source image pixel-wise classification. *Knowledge-Based Systems*, *221*, 106921. doi: 10.1016/j.knosys.2021.106921

Lu, W., Tao, C., Li, H., Qi, J., & Li, Y. (2022). A unified deep learning framework for urban functional zone extraction based on multi-source heterogeneous data. *Remote Sensing of Environment*, *270*, 112830. doi: 10.1016/j.rse.2021.112830

Malgwi, M. B., Fuchs, S., & Keiler, M. (2020). A generic physical vulnerability model for floods: Review and concept for data-scarce regions. *Natural Hazards and Earth System Sciences*, *20*(7), 2067–2090. doi: 10.5194/nhess-20-2067-2020

Met Office. (2006). MIDAS: UK Sub-hourly Rainfall Data. Retrieved 6 March 2024, from https://catalogue.ceda.ac.uk/uuid/455f0dd48613dada7bfb0ccfcb7a7d41

Okolie, C. J., & Smit, J. L. (2022). A systematic review and *meta*-analysis of Digital elevation model (DEM) fusion: Pre-processing, methods and applications. *ISPRS Journal of Photogrammetry and Remote Sensing*, *188*, 1–29. doi: 10.1016/j.isprsjprs.2022.03.016

Rahman, M. A., & Wang, Y. (2016). Optimizing Intersection-Over-Union in Deep Neural Networks for Image Segmentation. In G. Bebis, R. Boyle, B. Parvin, D. Koracin, F. Porikli, S. Skaff, … T. Isenberg (Eds.), *Advances in Visual Computing* (pp. 234–244). Cham: Springer International Publishing. doi: 10.1007/978-3-319-50835-1_22

Rees, W. G. (2000). The accuracy of Digital Elevation Models interpolated to higher resolutions. *International Journal of Remote Sensing*, *21*(1), 7–20. doi: 10.1080/014311600210957

https://doi.org/10.5194/nhess-2024-207
Preprint. Discussion started: 18 November 2024

Shang, C., Li, X., Foody, G. M., Du, Y., & Ling, F. (2022). Superresolution Land Cover Mapping Using a Generative Adversarial Network. *IEEE Geoscience and Remote Sensing Letters*, *19*, 1–5. doi: 10.1109/LGRS.2020.3020395

Shen, R., Huang, A., Li, B., & Guo, J. (2019). Construction of a drought monitoring model using deep learning based on multi-source remote sensing data. *International Journal of Applied Earth Observation and Geoinformation*, *79*, 48–57. doi: 10.1016/j.jag.2019.03.006

Tabari, H. (2020). Climate change impact on flood and extreme precipitation increases with water availability. *Scientific Reports*, *10*(1), 13768. doi: 10.1038/s41598-020-70816-2

Tan, W., Qin, N., Zhang, Y., McGrath, H., Fortin, M., & Li, J. (2024). A rapid high-resolution multi-sensory urban flood mapping framework via DEM upscaling. *Remote Sensing of Environment*, *301*, 113956. doi: 10.1016/j.rse.2023.113956

Tang, C. S. C., & Cheung, S. P. Y. (2011). *Frequency Analysis of Extreme Rainfall Values* (No. GEO Report No. 261; p. 209 p.). Civil Engineering and Development Department, HKSAR Government. Retrieved from Civil Engineering and Development Department, HKSAR Government website: https://www.cedd.gov.hk/eng/publications/geo/geo-reports/geo_rpt261/index.html

Wang, P., Bayram, B., & Sertel, E. (2022). A comprehensive review on deep learning based remote sensing image super-resolution methods. *Earth-Science Reviews*, *232*, 104110. doi: 10.1016/j.earscirev.2022.104110

Wang, Y., Chen, A. S., Fu, G., Djordjević, S., Zhang, C., & Savić, D. A. (2018). An integrated framework for high-resolution urban flood modelling considering multiple information sources and urban features. *Environmental Modelling & Software*, *107*, 85–95. doi: 10.1016/j.envsoft.2018.06.010

Wang, Y., Meng, F., Liu, H., Zhang, C., & Fu, G. (2019). Assessing catchment scale flood resilience of urban areas using a grid cell based metric. *Water Research*, *163*, 114852. doi: 10.1016/j.watres.2019.114852

Wang, Y., Zhang, C., Chen, A. S., Wang, G., & Fu, G. (2023). Exploring the relationship between urban flood risk and resilience at a high-resolution grid cell scale. *Science of The Total Environment*, *893*, 164852. doi: 10.1016/j.scitotenv.2023.164852

Wang, Z., Chen, J., & Hoi, S. C. H. (2021). Deep Learning for Image Super-Resolution: A Survey. *IEEE Transactions on Pattern Analysis and Machine Intelligence*, *43*(10), 3365–3387. doi: 10.1109/TPAMI.2020.2982166

Wu, J., Zhong, B., Tian, S., Yang, A., & Wu, J. (2019). Downscaling of Urban Land Surface Temperature Based on Multi-Factor Geographically Weighted Regression. *IEEE Journal of Selected Topics in Applied Earth Observations and Remote Sensing*, *12*(8), 2897–2911. doi: 10.1109/JSTARS.2019.2919936

Xie, J., Fang, L., Zhang, B., Chanussot, J., & Li, S. (2022). Super Resolution Guided Deep Network for Land Cover Classification From Remote Sensing Images. *IEEE Transactions on Geoscience and Remote Sensing*, *60*, 1–12. doi: 10.1109/TGRS.2021.3120891

Yang, W., Zhang, X., Tian, Y., Wang, W., Xue, J.-H., & Liao, Q. (2019). Deep Learning for Single Image Super-Resolution: A Brief Review. *IEEE Transactions on Multimedia*, *21*(12), 3106–3121. doi: 10.1109/TMM.2019.2919431

https://doi.org/10.5194/nhess-2024-207
Preprint. Discussion started: 18 November 2024

Yue, L., Shen, H., Li, J., Yuan, Q., Zhang, H., & Zhang, L. (2016). Image super-resolution: The techniques, applications, and future. *Signal Processing*, *128*, 389–408. doi: 10.1016/j.sigpro.2016.05.002

Yue, L., Shen, H., Yuan, Q., & Zhang, L. (2015). Fusion of multi-scale DEMs using a regularized super-resolution method. *International Journal of Geographical Information Science*, *29*(12), 2095–2120. doi: 10.1080/13658816.2015.1063639

Zhang, X., Zhang, W., Guo, S., Zhang, P., Fang, H., Mu, H., & Du, P. (2023). UnTDIP: Unsupervised neural network for DEM super-resolution integrating terrain knowledge and deep prior. *International Journal of Applied Earth Observation and Geoinformation*, *122*, 103430. doi: 10.1016/j.jag.2023.103430

Zhang, Yifan, & Yu, W. (2022). Comparison of DEM Super-Resolution Methods Based on Interpolation and Neural Networks. *Sensors*, *22*(3), 745. doi: 10.3390/s22030745

Zhang, Yulun, Li, K., Li, K., Wang, L., Zhong, B., & Fu, Y. (2018). Image Super-Resolution Using Very Deep Residual Channel Attention Networks. *arXiv:1807.02758 [Cs]*. Retrieved from http://arxiv.org/abs/1807.02758

Zhou, A., Chen, Y., Wilson, J. P., Chen, G., Min, W., & Xu, R. (2023). A multi-terrain feature-based deep convolutional neural network for constructing super-resolution DEMs. *International Journal of Applied Earth Observation and Geoinformation*, *120*, 103338. doi: 10.1016/j.jag.2023.103338

Zhou, A., Chen, Y., Wilson, J. P., Su, H., Xiong, Z., & Cheng, Q. (2021). An Enhanced Double-Filter Deep Residual Neural Network for Generating Super Resolution DEMs. *Remote Sensing*, *13*(16), 3089. doi: 10.3390/rs13163089

Zhu, Y., Geiß, C., & So, E. (2021). Image super-resolution with dense-sampling residual channel-spatial attention networks for multi-temporal remote sensing image classification. *International Journal of Applied Earth Observation and Geoinformation*, *104*, 102543. doi: 10.1016/j.jag.2021.102543